Photoionization dynamics of the NO $A\ ^2\Sigma^+$ state deduced from energy- and angle-resolved photoelectron spectroscopy

Hongkun Park and Richard N. Zare
Department of Chemistry, Stanford University, Stanford, California 94305

(Received 25 June 1993; accepted 19 July 1993)

The direct photoionization process NO $A\ ^2\Sigma^+$ $(v=0, N=13) \rightarrow NO^+ X\ ^1\Sigma^+$ $(v^+=0, N^+)+e^-$ is studied by energy- and angle-resolved photoelectron spectroscopy by employing two-color resonance-enhanced multiphoton ionization (REMPI) via excitation of the NO A–$X(0$–$0)$ $R_{21}(11.5)$ transition. The photoelectron angular distributions (PADs) associated with individual rotational levels N^+ of the ion are determined. Combined analysis of the newly obtained PADs and those reported earlier for the processes NO $A\ ^2\Sigma^+$ $(v=0, N\geqslant 20) \rightarrow NO^+ X\ ^1\Sigma^+$ $(v^+=0, N^+)+e^-$ via $P_{21}+Q_1$ branch excitation shows that the photoionization dynamics is independent of the rotational quantum number of state to be ionized and of the spin state of the photoelectron. Quantitative comparison of our results with threshold photoelectron measurements provides strong evidence that ionization in the pulsed-electric-field threshold technique is not via direct photoionization.

I. INTRODUCTION

Photoionization of a diatomic molecule AB (v, J) $+h\nu \rightarrow AB^+(v^+,N^+)+e^-$ may be regarded as a half-collision and a particularly simple example of photofragmentation. By preparing the AB molecule in a specific vibration–rotation level (v,J) with a known M_J state distribution, and by measuring the photoelectron angular distributions (PADs) associated with production of each vibration–rotation level (v^+,N^+) of the AB^+ ion, we have shown that it is possible to deduce the magnitudes and relative phase shifts of the electric dipole moment matrix elements that connect the photoelectron partial waves to the ionizing state.[1–4] Indeed, this information, which is almost tantamount to determining all the quantum numbers before and after this scattering process, constitutes essentially a "perfect" experiment.[5] To date, this procedure has been applied only to the photoionization of the NO $A\ ^2\Sigma^+$ $(v_i=0, N_i\geqslant 20)$ levels[3,4] although many photoelectron spectroscopic studies of small molecules have already achieved the resolution of the vibration–rotation levels of the ions.[6–9]

An underlying assumption in obtaining the dynamical information about the photoionization of the NO A state from previous experiments has been that the photoionization dynamics is independent of the rotational quantum number of the ionizing state.[4] This assumption is essentially the Born–Oppenheimer approximation applied to the *direct* photoionization dynamics, which reflects the disparity in time scales of electronic vs nuclear motions involved in the process. The classical angular frequency for a rotating diatomic molecule with rotational quantum number N is given by

$$\omega_{\rm rot}=4\pi Bc[N(N+1)]^{1/2}, \tag{1}$$

where B is the rotational constant and c is the speed of light. For NO $A\ ^2\Sigma^+$ $(v_i=0, N_i=13)$, as an example, $\omega_{\rm rot}$ is calculated to be 1.0×10^{13} rad/s, which corresponds to a tangential velocity of oxygen of 570 m/s. For NO $A\ ^2\Sigma^+$ $(v_i=0, N_i=25)$, the corresponding quantities are 1.9×10^{13} rad/s and 1080 m/s, respectively. In contrast, the velocity of a photoelectron ejected from the A state, which has an asymptotic energy of approximately 200 meV (the energy of photoelectrons detected in our experiments), is calculated to be 1.5×10^6 m/s at the point of departure from the ion core, assuming the radius of the NO A state to be 230 pm (the van der Waals radius for sodium) and zero orbital angular momentum for the photoelectron. These simplistic calculations show that the time scales for electronic and rotational motions are widely different and suggest that it is reasonable to assume that the photoionization dynamics is independent of the rotational quantum number in direct photoionization.

Previous studies also used the assumption that the photoionization dynamics is independent of photoelectron spin, although measurements of spin polarization were not performed.[4] This assumption was inferred from the very high degree of spin uncoupling in the NO A state as evidenced by the small spin–rotation coupling constant.[10,11] Good agreement between experimental data and *ab initio* calculations that employed the same assumption[12] added support for this notion. Considering the recent attention directed to the subject of spin polarization in theory and experiments,[13–15] a test of this assumption is desirable.

In this paper, we extend our previous studies and report rotationally resolved PADs for the $(1+1')$ REMPI process NO $X\ ^2\Pi$ $(v_g=0, J_g=11.5) \rightarrow$ NO $A\ ^2\Sigma^+$ $(v_i=0, N_i=13) \rightarrow NO^+X\ ^1\Sigma^+$ $(v^+=0, N^+)+e^-$ by employing linearly polarized excitation and ionization laser beams. By comparing the PADs with previous experimental data that were restricted to photoionization events for NO $A\ ^2\Sigma^+$ $(v_i=0, N_i\geqslant 20)$, we test the assumption of rotational-state independence of the direct photoionization dynamics. Excitation of the A–X R_{21} branch members employed here accesses F_2 spin–rotation levels, whereas excitation of the $P_{21}+Q_1$ branch members employed in previous works accesses predominantly the F_1 spin–rotation levels. Consequently, the current study also provides a test of the in-

 0021-9606/93/99(9)/6537/8/$6.00

volvement of spin dynamics. Finally, we compare the rotationally resolved photoelectron spectra obtained in our experiments with those obtained using the threshold photoelectron spectroscopic technique and offer arguments that the threshold photoelectrons are produced by a different ionization mechanism.

II. EXPERIMENT

The experimental apparatus is described in detail elsewhere[1,2] and only the details pertinent to this experiment are described here. The main component of our time-of-flight (TOF) photoelectron spectrometer is a magnetically shielded, field-free flight tube. The photoelectrons are generated by intersecting a molecular beam of NO with two counterpropagating pulsed laser beams at right angles. The electrons ejected in the direction mutually orthogonal to the laser beams and the molecular beam are detected using a microchannel plate located 51 cm from the intersection region.

The two colors λ_1 and λ_2 were obtained from Nd:YAG pumped pulsed dye lasers (DCR-1 and PDL-1, GCR-3 and PDL-3; Spectra-Physics) operating at a repetition rate of 10 Hz. The excitation color ($\lambda_1=225.6$ nm) was generated by frequency doubling the dye laser output (PDL-3) using a β-barium borate (BBO) crystal. The ionization color ($\lambda_2=307.2$ nm) was generated by frequency doubling the dye laser output (PDL-1) using a potassium dihydrogen phosphate (KDP) crystal. The excitation light beam was tuned to the $R_{21}(11.5)$ transition in the NO $A\,^2\Sigma^+$–$X\,^2\Pi$ (0–0) band. Both lasers were unfocused. The energies of the excitation and ionization light beams were $\sim$200 nJ/pulse and $\sim$50 μJ/pulse, respectively. The measurement of photoelectron signal vs excitation and ionization laser powers demonstrated no detectable saturation of excitation or ionization transition under the conditions employed in this study. Both the excitation and ionization laser beams were passed through zero-order quartz half-wave plates (Special Optics) mounted on stepper-motor-driven rotation stages which allowed independently rotatable polarizations.

In the experiment reported here, photoelectrons were found to be retarded by $\sim$70 meV because of stray electric or magnetic fields or both. Gold plating of the mu-metal flight tube, along with frequent cleaning and graphite coating, helped reduce, but did not eliminate the observed retardation of photoelectrons. For this reason, the photoelectron spectrometer was calibrated using the $(1+1')$ REMPI of NO employing the NO A–X (0–0) $P_{21}+Q_1(22.5)$ transition studied previously.[4] The detection efficiency of the experiment was found to be constant over the range of photoelectron kinetic energies measured in this experiment through the study of photoelectron intensity vs ionization laser wavelength. Our TOF spectrometer gave an energy resolution of $\sim$2 meV, which is sufficient to resolve single rotational levels of NO^+ for values of $N^+ \geqslant 10$.

A typical photoelectron TOF spectrum is shown in Fig. 1. Fully resolved photoelectron peaks are easily discernible in the spectrum; they correspond to production of

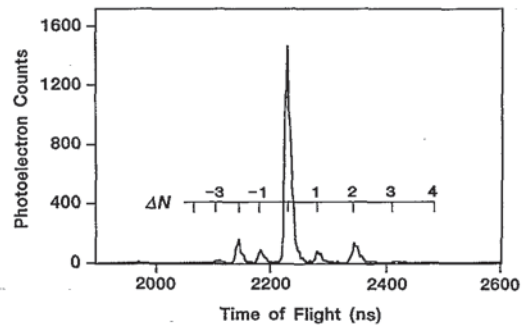

FIG. 1. The time-of-flight photoelectron spectrum of the $(1+1')$ REMPI process NO $X\,^2\Pi$ $(v_g=0,\ J_g=11.5)\rightarrow A\,^2\Sigma^+$ $(v_i=0,\ N_i=13)\rightarrow NO^+\ X\,^1\Sigma^+(v^+=0,\ N^+)+e^-$. The full width at half-maximum (FWHM) of each peak is 2 meV. Here, $\Delta N=N^+-N_i$.

ions in different rotational levels of $NO^+X\,^1\Sigma^+(v^+=0)$, denoted by $\Delta N=N^+-N_i$. Although $\Delta N=\pm 4$ transitions are possible in principle, they are not observed in the photoelectron spectrum. Almost symmetric intensity patterns for $\Delta N>0$ and $\Delta N<0$ transitions with the same $|\Delta N|$ value are also apparent. A typical angular distribution consisted of 50 000 laser shots per wave plate position, i.e., per detection angle θ, and included eight angles spanning two quadrants. Our experiments were performed with two different angles θ_T held between the excitation- and ionization-laser polarization vectors; $\theta_T=3°$ and $\theta_T=93°$. Details of our data acquisition method are given elsewhere.[1]

The experimental data reflect three types of errors. A small number of background photoelectrons arose from the scattered 225.6 nm radiation and from scattered signal photoelectrons. This contribution was reduced significantly by placing a baffle halfway inside the flight tube. The second type of error is from the inherent binomial statistics of photoelectron counting, which gives statistical errors approximately equal to the square root of the number of photoelectrons observed. For the experimental data reported here, this uncertainty dominated the background signal in the data. The third type of error, which is most difficult to quantify, is the systematic error that can be attributed to small deviations from ideal polarization quality of the two light beams and to minor deviations in the beam path that arise from rotation of the wave plates. Although great care was taken to reduce this systematic error, we could not eliminate it completely (we estimate it to be less than 5% of the intensity from careful inspection of our data). Whereas the fraction of statistical error to the photoelectron signal decreases as the number of photoelectron counts increases, the systematic error accumulates and becomes increasingly significant compared with other types of errors as the number of counts increases. Because this systematic error depends on experimental conditions and cannot be quantified exactly, it is not included in our data analysis.

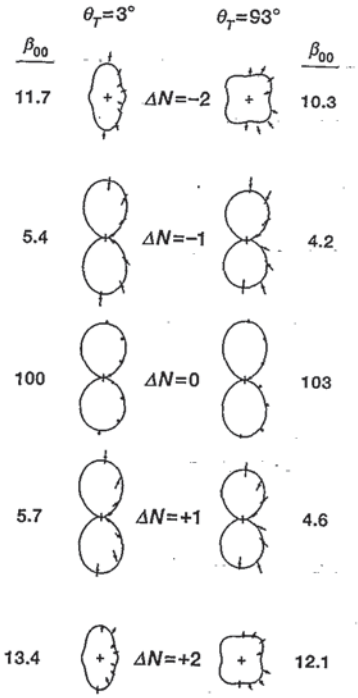

FIG. 2. Polar plots of the experimental photoelectron angular distributions (PADs) for excitation via the NO A–X (0–0) $R_{21}(11.5)$ transition. The plots are scaled to uniform size. The angle-integrated relative cross sections β_{00} are listed with PADs. The error bars represent 2σ uncertainties. The solid lines are the predictions of the model based on the results of the fit shown in Table II.

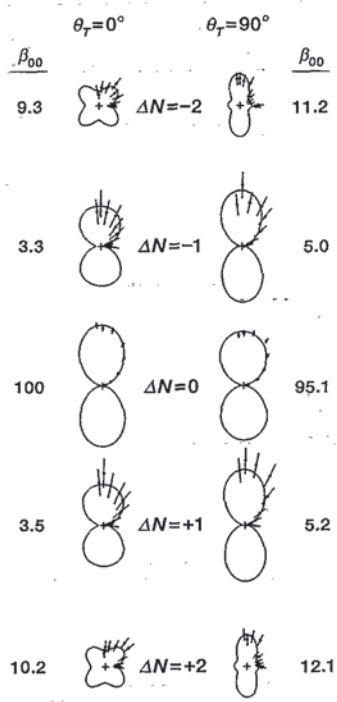

FIG. 3. Polar plots of the experimental photoelectron angular distributions (PADs) for excitation via the NO A–X (0–0) $P_{21}+Q_1(25.5)$ transition. The plots are scaled to uniform size. The angle-integrated relative cross sections β_{00} are listed with PADs. The error bars represent 2σ uncertainties. The solid lines are the predictions of the model based on the results of the fit shown in Table II.

III. RESULTS AND DISCUSSION

A. Experimental results and extraction of dynamical parameters

In Fig. 2, we show polar plots of the experimental PADs for five ion rotational states that result from the photoionization of NO $A\,^2\Sigma^+$ ($v_i=0$, $N_i=13$). The PADs shown in Fig. 2 have less dramatic nodal patterns than previously reported PADs employing a $P_{21}+Q_1$ branch transition shown in Fig. 3.[1] This difference is especially apparent for the $\Delta N=\pm 2$ transitions. The rotationally resolved PADs from $(1+1')$ REMPI have previously been shown both theoretically[16,17] and experimentally[1,2] to be sensitive to intermediate-state alignment and photoionization dynamics. The high degree of alignment facilitates preferential probing of parallel or perpendicular ionization moments with respect to the molecular axis by choice of θ_T.

The most appropriate way to examine the degree of alignment in the intermediate state generated in the excitation step is to describe the alignment in terms of state multipoles $T(K,Q)$.[18,19] The monopole $T(0,0)$ is a scalar and serves as a normalization constant. The quadrupole tensor $T(2,Q)$ represents alignment. When Q is nonzero, $T(K,Q)$ describes coherence among the magnetic sublevels. The state multipole of rank K and component Q for the intermediate state in the frame in which the direction of the ionization laser polarization is set to be the Z axis is given by[17,18]

$$T(K,Q;\theta_T)=\sum_{M_{N_i},M'_{N_i}}(-1)^{N_i-M_{N_i}}(2K+1)^{1/2}\times\begin{pmatrix}N_i & N_i & K\\ M_{N_i} & -M'_{N_i} & Q\end{pmatrix}^{N_i}\rho_{M_{N_i},M'_{N_i}}(\theta_T). \quad (2)$$

The definitions of quantum numbers that appear throughout this paper follow those in Table I of Ref. 17. An expression for the density matrix elements is also given in Ref. 17. Note that $T(K,Q;\theta_T)$ depends on θ_T in addition to the rotational branch employed in the experiment because of the frame rotation involved when linear polarization vectors of the excitation and ionization lasers are not parallel. Table I lists values of $T(2,Q;\theta_T)/T(0,0;\theta_T)$ calculated for the intermediate level $N_i=13$ following $R_{21}(11.5)$ excitation with $\theta_T=3°$ and $\theta_T=93°$. Also listed, for comparison, are the corresponding values calculated for the intermediate rotational quantum number $N_i=25$ following $P_{21}+Q_1(25.5)$ excitation with $\theta_T=0°$ and $\theta_T=90°$. Because the preparation of the intermediate states involves only one linearly polarized photon, we need to consider only the state multipoles with rank 0 and 2 under the approximation of a weak-field electric-dipole transition. When $\theta_T=0°$, in which case the cylindrical symmetry is preserved, the values of $T(2,Q\neq 0;\theta_T)$ should be zero. When $\theta_T=90°$, the reflection symmetry is preserved and the values of $T(2,Q=\pm 1;\theta_T)$ are zero. Table I reveals immediately that excitation of the $R_{21}(11.5)$ transition generates less alignment in the intermediate state than does

TABLE I. State multipoles for the intermediate level NO $A\,^2\Sigma^+$ ($v_i=0$, N_i) following the transitions given in the top row at laser geometries described by the angle θ_T. The values of N_i accessed through the $R_{21}(11.5)$ transition and the $P_{21}+Q_1(25.5)$ transition are 13 and 25, respectively.

	NO $A\,^2\Sigma^+$–$X\,^2\Pi$ transition			
	$R_{21}(11.5)$		$P_{21}+Q_1(25.5)$	
Normalized state multipole	$\theta_T=3°$	$\theta_T=93°$	$\theta_T=0°$	$\theta_T=90°$
$T(2,0;\theta_T)/T(0,0;\theta_T)$	−0.498	0.248	0.751	−0.375
$T(2,2;\theta_T)/T(0,0;\theta_T)$	−0.001	−0.305	0.000	0.460
$T(2,-2;\theta_T)/T(0,0;\theta_T)$	−0.001	−0.305	0.000	0.460
$T(2,1;\theta_T)/T(0,0;\theta_T)$	0.032	−0.032	0.000	0.000
$T(2,-1;\theta_T)/T(0,0;\theta_T)$	−0.032	0.032	0.000	0.000

the $P_{21}+Q_1(25.5)$ transition for both $\theta_T\sim0°$ and $\theta_T\sim90°$. This reduction in the degree of alignment explains why the rotationally resolved PADs in this experiment have less marked nodal patterns than observed previously.

We attempted to fit the observed rotationally resolved PADs to the model we reported previously[17] to obtain the dynamical parameters that describe the photoionization dynamics of the NO A state. The fitting parameters in the model represent the magnitudes ($r_{l\lambda}$) and phase shifts ($\eta_{l\lambda}$) of the vibrationally averaged radial electric dipole matrix elements that connect the electronic wave function of the NO A state to the outgoing photoelectron partial waves with orbital angular momentum l and the projection of l on the internuclear axis λ,

$$r_{l\lambda}e^{i\eta_{l\lambda}}=\int \chi^+_{\rm vib}(R)\left\langle \Psi^+_{\rm elec}[(r_s);R]\Psi_{l\lambda}(\mathbf{k};R)\right|\sum_s r_s Y_{1\mu_\lambda}(\hat{r}_s)\times\left|\Psi^i_{\rm elec}[(r_s);R]\right\rangle\chi^i_{\rm vib}(R)dR. \tag{3}$$

As before, the Levenberg–Marquadt modified nonlinear least-squares method was used in the fitting procedure.[20] The fitting was decomposed into two independent parts, taking advantage of the selection rule $\Delta N+l=$odd that is applicable in the photoionization of the NO $A\,^2\Sigma^+$ state[21,22]; the $\Delta N=0,\ \pm2,\ \pm4$ ionizing transitions were fit with parameters for the odd l waves, and $\Delta N=\pm1,\pm3$ ionizing transitions were fit with parameters for the even l waves. Although we did not observe $\Delta N=\pm4$ transitions experimentally, the explicit inclusion of this information in the data set provided additional constraints in the fitting procedure and improved the convergence of the fit. The selection rule mentioned above simplifies the fitting procedure significantly, but at the same time prohibits us from determining the phase relationship between the even and odd partial waves. In addition, the PADs are insensitive to the overall phase of the outgoing partial waves. Hence, we are free to set $\eta_{s\sigma}\equiv\eta_{p\sigma}\equiv0$ in the fit. The partial wave expansion was truncated at $l=3$.[1] In the fit, F_l and Γ_l, which are defined by

$$F_l\equiv r^2_{l\sigma}+2r^2_{l\pi} \tag{4}$$

and

$$\Gamma_l\equiv\frac{r^2_{l\sigma}}{r^2_{l\sigma}+2r^2_{l\pi}}; \tag{5}$$

were used as fitting parameters along with $\eta_{l\lambda}$. F_l represents the fraction of l character contributing to the outgoing photoelectron wave and Γ_l represents the fraction of σ character in a given l wave.

Previous studies showed that these parameters gave a much less correlated fit than the one obtained by using $r_{l\lambda}$.[1,2] In a highly correlated fit, the fitting parameters do not vary independently in the fitting procedure, which makes the physical interpretations of fitting parameters ambiguous. We found, however, that significant correlations between various fitting parameters still existed when we tried to fit the present R_{21} branch data alone, although we used the above-defined parameters. Actually the correlations were much larger than those found in the previous studies. For instance, the correlation coefficients between F_s and F_d and between F_f and Γ_p were found to be −0.99 and 0.87, respectively. These strong anticorrelations and correlations between parameters generated artificially high uncertainties in the fit, which prevented us from obtaining a reliable determination of some of these dynamical parameters. The increased correlation between various fitting parameters is at least partly caused by the reduced alignment in the intermediate state noted above. This reduced alignment results in the diminished nodal patterns in the observed rotationally resolved PADs, which makes a figure-of-merit function in the fit (the chi square in our case) less sensitive to the variations of fitting parameters. This behavior has also been observed previously.[1] The values of the dynamical parameters were, however, quite similar to those reported previously within the uncertainties of the fit. The only significantly different parameters were Γ_p and $\eta_{p\pi}$, and they were strongly correlated with other parameters.

Although strong correlations exist between parameters, the results of the fit seem to support the conjecture that the photoionization dynamics is independent of the rotational quantum number of the ionizing states in the direct photoionization of the NO $A\,^2\Sigma^+$ ($v_i=0$) state. Indeed, when we plotted the experimentally determined PADs for $N_i=13$ with theoretical predictions based on dynamical parameters reported previously from $N_i\geqslant20$ data,[4] we found the theoretical lines to match the experimental PADs quite well.

Prompted by these observations, we performed a simultaneous nonlinear least-squares fitting of all the experimental data available to us. Included in this fit were the rotationally resolved PADs from the $(1+1')$ REMPI via NO A–$X(0$–$0)$ $P_{21}+Q_1(25.5)$ excitation employing linearly polarized excitation and ionization beams,[1] those via NO A–$X(0$–$0)$ $P_{21}+Q_1(22.5)$ excitation employing linearly polarized excitation and circularly polarized ionization beams,[4] and finally the newly obtained PADs via NO A–$X(0$–$0)$ $R_{21}(11.5)$ excitation employing linearly polarized excitation and ionization beams. The current experimental data set consists of more photoelectron counts than the two data sets reported previously did, which

TABLE II. Parameters resulting from the fit of experimental data for photoionization of NO via the $A\,^2\Sigma^+$ ($v=0$) state. Also shown are the results of the *ab initio* calculation of Rudolph and McKoy (Ref. 12). F_l values are normalized so that they sum to unity. The values in parentheses represent 1σ uncertainties in the fit.

Parameter	Fit	*Ab initio*[a]
F_s	0.040 (0.003)	0.025
F_p	0.702 (0.005)	0.653
F_d	0.040 (0.002)	0.050
F_f	0.218 (0.004)	0.272
Γ_p	0.28 (0.02)	0.119
Γ_d	0.69 (0.05)	0.984
Γ_f	0.45 (0.05)	0.471
$\delta_{p\pi-p\sigma}$	+13° (1°)	+9.8°
$\delta_{d\pi-d\sigma}$	−70° (10°)	+93.3°
$\delta_{f\pi-f\sigma}$	+2° (9°)	−1.6°
$\delta_{d\sigma-s\sigma}$	−154° (8°)	+173.7°
$\delta_{f\sigma-p\sigma}$	−70° (7°)	−76.3°

[a]The phase factors i^l and $(-1)^\lambda$ have been removed from the phases given in Ref. 12 for comparison with our fit results.

makes the statistical error bars two to three times smaller than those reported earlier. As a consequence, the effective weight given to the R_{21} branch data set is greater than those given to the other two data sets in the fit. This differential weighting among data sets is not favorable considering the relatively featureless nature of the R_{21} branch data set and especially the systematic errors in the data set. Therefore, we increased the uncertainties in the R_{21} branch data set by a factor of 2, so that the weights given to all the data sets became comparable. This protocol is equivalent to reducing the number of photoelectron counts of the R data set.

The results of the fit are given in Table II. We list the phase shift differences $\delta_{l\lambda-l'\lambda'}=\eta_{l\lambda}-\eta_{l'\lambda'}$ instead of $\eta_{l\lambda}$ because $\delta_{l\lambda-l'\lambda'}$ are the quantities determined from the fit without arbitrariness. Note that the signs of $\delta_{l\lambda-l'\lambda'}$ are determined from the fit because of the inclusion of the data set employing the circularly polarized ionization beam.[3,4] Otherwise, $\delta_{l\lambda-l'\lambda'}$ would be double valued. Converting F_l and Γ_l values obtained from the fit to $r_{l\lambda}$ values is straightforward using Eqs. (4) and (5). The dynamical parameters listed in Table II are uniquely determined in the sense that they give a minimum chi-square value. The fit results presented in Table II agree very well with those reported previously (see Table I in Ref. 4) except for the value of Γ_p. Investigation of the correlation matrix from the fit showed that the correlations between fitting parameters were reduced significantly, which indicated that the fit results are more reliable than the fit results obtained using the R_{21} branch data only. The model PADs predicted by the dynamical parameters from the fit are shown as solid lines in Fig. 2. For comparison, the model PADs predicted by the same dynamical parameters for the $(1+1')$ REMPI via NO A–$X(0$–$0)$ $P_{21}+Q_1(25.5)$ excitation are given in Fig. 3 along with the experimental data presented previously.[1] The β_{00} values in Figs. 2 and 3 designate the angle-integrated relative cross sections for each ionizing transition.

B. Discussion of experimental results and comparison with *ab initio* calculations

Inspection of Figs. 2 and 3 shows that the experimental PADs from both the NO $A\,^2\Sigma^+$ ($v_i=0$, $N_i=13$) and $A\,^2\Sigma^+$ ($v_i=0$, $N_i=25$) levels agree very well with the theoretical predictions based on the dynamical parameters determined from the simultaneous fit of all the data. Although not shown, the experimental PADs obtained with circularly polarized ionization[4] are also found to agree very well with the theoretical predictions based on the same parameters.

Note that a *single* set of dynamical parameters suffices to describe photoionization experiments from different rotational levels. This observation is a strong indication that the photoionization dynamics from the NO A state is independent of the rotational quantum number in the intermediate state within our experimental accuracy. By the same token, it also indicates that the photoionization dynamics of the NO A state is independent of the photoelectron spin states, since the R_{21} branch excitation employed in this experiment accesses a different spin–rotation level (F_2) in the intermediate state from that accessed by $P_{21}+Q_1$ branch excitation (F_1) employed in previous experiments. Admittedly, we cannot exclude the possibility that the dynamical parameters that describe the photoionization dynamics from different rotational levels may vary slightly with the rotational quantum number and the electronic spin, but these variations should be small because we cannot detect them experimentally.

We emphasize that the present experiment is a very stringent test for the assumptions discussed above. In analyzing the experimental results reported here, we were able to separate photoionization dynamics from geometrical factors that affect the observed PADs, such as the effect of intermediate-state alignment. We note that the observed branching ratios in the rotationally resolved photoelectron spectra are a function of the rotational quantum number in the intermediate state. Therefore, the observations of the branching ratios for various ion rotational transitions alone do not give sufficient information to confirm the above-mentioned assumptions. The rotationally resolved PADs, in contrast, provide a key test for these assumptions. The disentanglement of the effect of intermediate-state alignment is also invaluable in this regard.

Our interpretation of the photoionization dynamics for the system NO $A\,^2\Sigma^+$ $(v_i=0)\rightarrow NO^+$ $X\,^1\Sigma^+$ $(v^+=0)$ $+e^-$ remains almost the same as before. The photoionization cross section is dominated by the contribution from the p partial wave, which is consistent with the description of the NO $A\,^2\Sigma^+$ state as a $3s\sigma$ Rydberg state. The precise determination of the degree of the σ character of the p wave, which is represented by Γ_p, is somewhat problematic because the value of it in the fit that includes the new data set differs somewhat from that in the previous fit *(vide infra)*. The newly determined value for Γ_p indicates that the p wave has slightly more π character than σ character, whereas the previous value indicates almost no preference for σ or π character. A significant fraction of f-wave character in the partial wave continua exists that indicates the

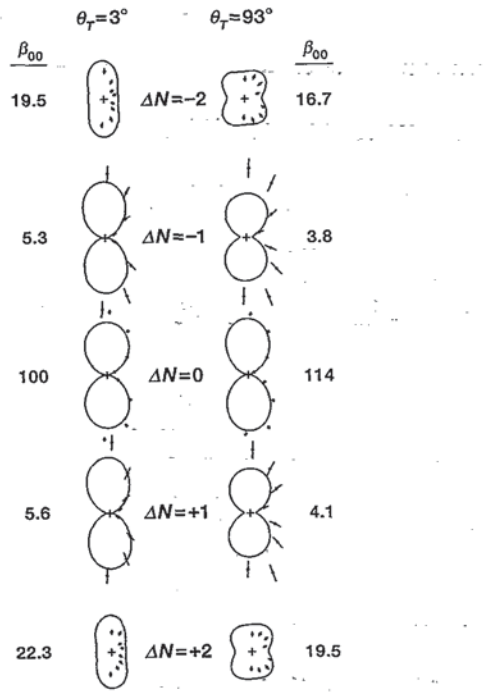

FIG. 4. A comparison of the experimental photoelectron angular distributions (PADs) for excitation via the NO A–X (0–0) $R_{21}(11.5)$ transition (data points with 2σ error bars) with the *ab initio* predictions (solid lines) of Rudolph and McKoy (Ref. 12). The scaling of the *ab initio* results to the experimental PADs was performed such that the total ionization cross section was equal for the two cases.

scattering of ejected photoelectrons by interaction with the quadrupole moment of the ion core. The dipolar interaction between the photoelectron and the molecular ion should not be large, as evidence by the small partial cross sections for the s and d waves.

In the last column of Table II, we list the *ab initio* dynamical parameters calculated by Rudolph and McKoy.[12] The dynamical parameters determined in our fit and from the *ab initio* calculation can be compared directly. The theoretical formalism behind our fitting equations depends heavily on the work of Dixit and McKoy,[23] which also formed the basis for the *ab initio* calculation. In general, good agreement is found. Several discrepancies exist, however. The best way to illustrate these discrepancies is to show the rotationally resolved PADs that are calculated using *ab initio* parameters for individual ionizing transitions. The results for the $(1+1')$ REMPI via NO A–X(0–0) $R_{21}(11.5)$ excitation are shown in Fig. 4, along with our experimental data. The calculated PADs were scaled so that the total ionization cross section was equal to that of experimental data. We can see immediately that the *ab initio* parameters do not yield satisfactory PADs and rotational branching ratios in contrast to the dynamical parameters obtained from our fit (cf. Figs. 2 and 4). Although they are not shown here, the corresponding comparisons for the other experimental data yield similar degrees of disagreement.

At this point, we discuss the uniqueness of our fit. We noted earlier that the comparison of the dynamical parameters obtained here with those reported previously showed a slight differences in Γ_p values. The results obtained from the R_{21} branch data alone did not agree completely with the results of the simultaneous fit. They also exhibited extensive correlations between fitting parameters. These observations may raise questions about the uniqueness and accuracy of our fit in representing physically meaningful dynamical parameters. The convergence of our fit is determined by minimization of the chi square. The fact that we obtained the lowest chi-square value does not guarantee, however, that the parameters determined in the fit really correspond to the true physical parameters, especially when there are systematic errors involved. Careful examination indicates that there is a region of the F–Γ–η parameter space, involving the correlated variations of several parameters, such as Γ_p and $\delta_{p\pi-p\sigma}$, that can describe the experimental data acceptably. Because this region is found to be a very small fraction of the total parameter space, we are assured that the parameters in Table II are still a good representation of true dynamical parameters that describe photoionization of the NO A state with asymptotic photoelectron energies around 200 meV.

The comparison of Fig. 2 with Fig. 4 serves as a good example of this conclusion. Although the overall differences in the *ab initio* parameters and the parameters from our fit are small, the resulting PADs show quite dramatic differences in shape and branching ratio. We hesitate, however, to ascribe this disagreement to differences in specific dynamical parameters because of the correlation among parameters in our fit mentioned above.

The failure of the *ab initio* calculation to accurately describe the rotationally resolved PADs, and thus, the photoionization dynamics of the NO A state, suggests that the *ab initio* calculation could be improved. Recall, however, that the underlying physics is well represented by the *ab initio* calculation. The detail of the comparison between our experiments and the *ab initio* calculation is unprecedented. Although most comparisons between experiment and theory performed so far involved quantities such as integral reaction cross section[24] or partially resolved differential cross sections,[25] the comparison here involves fully state-specific differential cross sections for the half-collision of $NO^+ + e^-$. Despite this degree of detail, our experimental results and the *ab initio* results generally agree well. Even the signs of the relative scattering phases agree in most instances. We believe that the quantitative description of this system will serve as a challenge to *ab initio* calculations directed toward describing the photoionization of small molecules.

C. Comparison with threshold photoelectron experiments

The photoionization of the NO A state has been studied extensively using threshold photoelectron techniques, which are often referred to as zero-kinetic-energy photoelectron spectroscopy (ZEKE).[26–31] The experiments usually involve pulsed-field ionization (PFI) of the high-lying Rydberg state(s) accessed through the NO $A\,^2\Sigma^+$ ($v_i=0$, $N_i<10$) levels, and show superior photoelectron energy

resolution compared with experiments in which conventional photoelectron spectroscopic techniques are used. Interestingly, however, the negative ΔN transitions are observed to have higher intensity than the positive ΔN transitions in these ZEKE spectra, which is in sharp contrast to our experimental findings and the results of an *ab initio* calculation[32] that the negative and positive ΔN transitions for the same value of $|\Delta N|$ are almost symmetric in intensity (Figs. 2 and 3). The slight differences in branching ratios for positive and negative ΔN transitions in our spectra can be attributed to differences in geometric factors that reflect the larger number of open M_N channels involved in $\Delta N>0$ transitions than in $\Delta N<0$ transitions. The above trend is not restricted to the ZEKE spectra of the NO A state, but is rather general in most of the ZEKE spectra recorded to date.[33–36]

To make the comparison between the ZEKE observations and our experiments more quantitative, we calculated the ion rotational branching ratios for the $(1+1')$ REMPI via NO A–$X(0$–$0)$ $R_1(7.5)$ excitation[30,37] using the dynamical parameters determined from the fit. This calculation assumes that the dynamical parameters obtained in our experiments for the asymptotic photoelectron energy of approximately 200 meV can describe the threshold photoionization dynamics. Because theoretical calculations showed that the photoionization dynamics of the NO A state is not very sensitive to photoelectron energy,[38] we expect this assumption to be reasonable if, and only if, the ionization mechanisms in ZEKE and our experiments are the same. We also assume in this calculation that the photoionization of the NO $A\,^2\Sigma^+$ $(v_i=0, N_i=8)$ level can be described by the dynamical parameters for the photoionization of the NO $A\,^2\Sigma^+$ $(v_i=0, N_i>10)$ levels. The relative angle-integrated intensities calculated for each ionizing transition are 11.2, 5.4, 100, 5.8, and 13.9 for the $\Delta N=-2$, -1, 0, 1, and 2 transitions, respectively, when the excitation and ionization laser polarizations are set to be parallel. Here the intensity for the $\Delta N=0$ transition is arbitrarily fixed to be 100. The corresponding relative intensities observed experimentally from the ZEKE spectrum are 12, 16.2, 100, 9.7, and 14.0 in the same order as given above.[30]

We note that one study[29] reports PADs under "near-ZEKE" conditions. The reported angular acceptance of 29° and the smoothing of the data, however, severely limit comparison with our present results.

The comparison given above shows clearly that the experimentally observed ZEKE branching ratios and our predictions are different, especially for $\Delta N=\pm 1$ transitions. Our prediction shows no skew in the branching ratio favoring negative ΔN, whereas the ZEKE data do. More prominently, our prediction shows that $\Delta N=\pm 2$ transitions are stronger in intensity than $\Delta N=\pm 1$ transitions, whereas the ZEKE data show that the $\Delta N=-1$ transition is the strongest among the $\Delta N\neq 0$ transitions. These are strong indications that the ionization mechanism in the ZEKE experiment differs from that probed in our experiments, which we believe to be via direct photoionization.

The realization that the ionization mechanism in the ZEKE experiments is not via direct photoionization is not new. This idea has been proposed by several authors[30,39–42] who point out that rotational autoionization leads to strong perturbations of rotational line intensities in the ZEKE spectra. The presence of an electric field is known to effect the field-induced and/or forced-field autoionization through extensive l and J mixing,[39,40] which facilitates rotational autoionization. Another way that l and J mixing can be induced is through the inherent anisotropy of the molecular core, which is not spherical.[42] The enhanced rotational autoionization, in turn, results in highly skewed rotational line intensities which favor the negative ΔN transitions over positive ΔN transitions in ZEKE spectra. Although many theoretical attempts to explain the observed trends in ZEKE spectra exist, only a few comparisons have been made between ZEKE data and conventional photoelectron spectroscopic data. Merkt and Softley studied the ZEKE spectra of ground-state H_2 (Ref. 34) and N_2 (Ref. 35), and observed rotational branching ratios that differed from those obtained from corresponding conventional photoelectron spectra. They also found that the theoretical predictions assuming direct photoionization dynamics deviated from the ZEKE observations.

The comparison between ZEKE data and our data for the NO A state presented here shows the same qualitative trend as observed by Merkt and Softley,[34,35] and provides additional, convincing evidence that the photoionization dynamics under the ZEKE-PFI experimental conditions is not via direct photoionization. Moreover, the comparison given above provides a very intriguing observation that the disagreement between the ZEKE data and our prediction is much more prominent for $\Delta N=\pm 1$ transitions than for $\Delta N=\pm 2$ transitions. Because the s and d partial waves, which arise from the dipole-induced mixing of the partial waves in the direct photoionization, produce $\Delta N=\pm 1$ transitions, the above observation suggests that the generation of s and d waves may be facilitated under ZEKE experimental conditions caused perhaps by more s and d character being induced into the Rydberg states converging to the ionization continuum. The observation also suggests that the l mixing proposed to occur under ZEKE conditions does not yield uniformly distributed l distributions in the Rydberg continua of NO. Clearly, much more remains to be learned before the photoionization dynamics under PFI conditions can be fully specified, and we believe that caution should be exercised in interpreting the dynamical information obtained from ZEKE experiments.

IV. CONCLUSIONS

We have presented rotationally resolved PADs for the process NO $A\,^2\Sigma^+$ $(v_i=0, N_i=13)\rightarrow NO^+\,X\,^1\Sigma^+$ $(v^+=0, N^+)+e^-$. Through the combined analysis of our new data employing R_{21} branch excitation with the data previously reported employing $P_{21}+Q_1$ branch excitation, we observe that the *direct* photoionization dynamics is independent, within our experimental accuracy, of the rotational quantum number of a state to be ionized. This conclusion is consistent with the prediction based on the Born–Oppenheimer approximation. The dependence of the

photoionization dynamics on spin states of photoelectrons is also found to be undetectable in the case of the NO A state. The comparison between *ab initio* calculations and our experimental data shows good overall agreement between theory and experiment, but also that the theoretical calculations should be improved to provide a more quantitative description of the photoionization of the NO A state. We have provided a quantitative comparison between our data and ZEKE data. We find that the ZEKE data for the NO A state are not consistent with a direct photoionization mechanism.

ACKNOWLEDGMENTS

We thank David J. Leahy and Katharine L. Reid for helpful discussions. We acknowledge the support of the National Science Foundation under Grant No. PHY 90-20457.

[1] S. W. Allendorf, D. J. Leahy, D. C. Jacobs, and R. N. Zare, J. Chem. Phys. **91**, 2216 (1989).
[2] D. J. Leahy, K. L. Reid, and R. N. Zare, J. Chem. Phys. **95**, 1757 (1991).
[3] K. L. Reid, D. J. Leahy, and R. N. Zare, Phys. Rev. Lett. **68**, 3527 (1992).
[4] D. J. Leahy, K. L. Reid, H. Park, and R. N. Zare, J. Chem. Phys. **97**, 4948 (1992).
[5] B. Bederson, Comments At. Mol. Phys. **1**, 41 (1969).
[6] W. G. Wilson, K. S. Viswanathan, E. Sekreta, and J. P. Reilly, J. Phys. Chem. **88**, 672 (1984).
[7] K. S. Viswanathan, E. Sekreta, E. R. Davidson, and J. P. Reilly, J. Phys. Chem. **90**, 5078 (1986).
[8] M. A. O'Halloran, S. T. Pratt, P. M. Dehmer, and J. L. Dehmer, J. Chem. Phys. **87**, 3288 (1987).
[9] E. de Beer, M. Born, C. A. de Lange, and N. P. C. Westwood, Chem. Phys. Lett. **186**, 40 (1991).
[10] A. Timmermann and R. Wallenstein, Opt. Commun. **39**, 239 (1981).
[11] R. J. Miller, W. L. Glab, and B. A. Bushaw, J. Chem. Phys. **91**, 3277 (1989).
[12] H. Rudolph and V. McKoy, J. Chem. Phys. **91**, 2235 (1989).
[13] N. A. Cherepkov, J. Phys. B **14** L73 (1981).
[14] N. Chandra, Phys. Rev. A **36**, 768 (1989).
[15] N. Böwering, M. Salzmann, M. Müller, H. -W. Klausing, and U. Heinzmann, Phys. Rev. A **45**, R11 (1992).
[16] H. Rudolph, S. N. Dixit, V. McKoy, and W. M. Huo, J. Chem. Phys. **88**, 1516 (1988).
[17] K. L. Reid, D. J. Leahy, and R. N. Zare, J. Chem. Phys. **95**, 1746 (1991).
[18] K. Blum, *Density Matrix Theory and Applications* (Plenum, New York, 1981).
[19] R. N. Zare, *Angular Momentum* (Wiley-Interscience, New York, 1988).
[20] W. H. Press, B. P. Flannery, S. A. Teukolsky, and W. T. Vetterling, *Numerical Recipes* (Cambridge University, London, 1986).
[21] S. N. Dixit and V. McKoy, Chem. Phys. Lett. **128**, 49 (1986).
[22] J. Xie and R. N. Zare, J. Chem. Phys. **93**, 3033 (1990).
[23] S. N. Dixit and V. McKoy, J. Chem. Phys. **82**, 3546 (1985).
[24] D. E. Adelman, N. E. Shafer, D. A. V. Kliner, and R. N. Zare, J. Chem. Phys. **97**, 7323 (1992).
[25] D. M. Neumark, A. M. Wodtke, G. N. Robinson, C. C. Hayden, and Y. T. Lee, J. Chem. Phys. **82**, 3045 (1985).
[26] K. Müller-Dethlefs, M. Sander, and E. W. Schlag, Chem. Phys. Lett. **112**, 291 (1984).
[27] M. Sander, L. A. Chewter, K. Müller-Dethlefs, and E. W. Schlag, Phys. Rev. A **36**, 4542 (1987).
[28] G. Reiser, W. Habenicht, K. Müller-Dethlefs, and E. W. Schlag, Chem. Phys. Lett. **152**, 119 (1988).
[29] G. Reiser, D. Rieger, and K. Müller-Dethlefs, Chem. Phys. Lett. **183**, 239 (1991).
[30] G. Reiser and K. Müller-Dethlefs, J. Phys. Chem. **96**, 9 (1992).
[31] M. Takahashi, H. Ozeki, and K. Kimura, Chem. Phys. Lett. **181**, 255 (1991).
[32] H. Rudolph, V. McKoy, and S. N. Dixit, J. Chem. Phys. **90**, 2570 (1989).
[33] G. P. Bryant, Y. Jiang, M. Martin, and E. R. Grant, J. Phys. Chem. **96**, 6875 (1992).
[34] F. Merkt and T. P. Softley, J. Chem. Phys. **96**, 4149 (1992).
[35] F. Merkt and T. P. Softley, Phys. Rev. A **46**, 302 (1992).
[36] R. G. Tonkyn, R. T. Wiedmann, and M. G. White, J. Chem. Phys. **96**, 3696 (1992).
[37] Although the NO A–X(0–0) $R_1(7.5)$ transition was reported to be used to prepare NO $A\,^2\Sigma^+$ (v_i=0, N_i=8) in Ref. 29, we believe that it is actually the NO A–X(0–0) $Q_{21}+R_1(7.5)$ excitation. We used, however, the reported branch designation $R_1(7.5)$ in our calculation. The qualitative arguments that follows are found not to be affected by the choice of the branch designation because the Q:R ratio in this mixed branch excitation is 1:4 based on relative rotational line strengths.
[38] H. Rudolph, S. N. Dixit, V. McKoy, and W. M. Huo, J. Chem. Phys. **88**, 637 (1988).
[39] W. A. Chupka, J. Chem. Phys. **98**, 4520 (1993).
[40] F. Merkt, H. H. Fielding, and T. P. Softley, Chem. Phys. Lett. **202**, 153 (1993).
[41] R. T. Wiedmann, M. G. White, K. Wang, and V. McKoy, J. Chem. Phys. **98**, 7673 (1993).
[42] U. Even and R. D. Levine (private communication).